HHS Public Access

Author manuscript

Mol Imaging Biol. Author manuscript; available in PMC 2017 June 17.

Published in final edited form as:

Mol Imaging Biol. 2016 April ; 18(2): 209–218. doi:10.1007/s11307-015-0878-9.

Intraoperative Molecular Imaging of Lung Adenocarcinoma Can Identify Residual Tumor Cells at the Surgical Margins

Jane J. Keating, M.D.[1], **Olugbenga T. Okusanya, M.D.**[1], **Elizabeth De Jesus, B.A.**[1], **Ryan Judy, B.A.**[1], **Jack Jiang, B.S.**[1], **Charuhas Deshpande, M.D.**[2], **Shuming Nie, Ph.D.**[3], **Philip Low, Ph.D.**[4], and **Sunil Singhal, M.D.**[1]

[1]Division of Thoracic Surgery, Department of Surgery, University of Pennsylvania and Philadelphia VA Medical Center, Philadelphia, PA

[2]Department of Pathology, University of Pennsylvania, Perelman School of Medicine, Philadelphia, PA

[3]Departments of Biomedical Engineering and Chemistry, Emory University, Atlanta, GA

[4]Department of Chemistry, Purdue University, West Lafayette, IN

Abstract

Purpose—During lung surgery, identification of surgical margins is challenging. We hypothesized that molecular imaging with a fluorescent probe to pulmonary adenocarcinomas could enhance residual tumor during resection.

Procedures—Mice with flank tumors received a contrast agent targeting folate receptor alpha. Optimal dose and time of injection was established. Margin detection was compared using traditional methods versus molecular imaging. A pilot study was then performed in 3 humans with lung adenocarcinoma.

Results—The peak tumor-to background ratio (TBR) of murine tumors was 3.9. Fluorescence peaked at 2 hours and was not improved beyond 0.1 mg/kg. Traditional inspection identified 30% of mice with positive margins. Molecular imaging identified an additional 50% of residual tumor deposits ($P<0.05$). The fluorescent probe visually enhanced all human tumors with a mean TBR of 3.5.

Conclusions—Molecular imaging is an important adjunct to traditional inspection to identify surgical margins after tumor resection.

Introduction

Non-small cell lung cancer (NSCLC) is the most common cancer killer in the United States and affects 220,000 people a year. Mechanically removing a localized lung cancer improves

*Corresponding Author: Sunil Singhal, Division of Thoracic Surgery, University of Pennsylvania School of Medicine, 6 White Building, 3400 Spruce Street, Philadelphia, PA 19104, sunil.singhal@uphs.upenn.edu.

Conflicts of Interest

Dr. Low is a consultant and stakeholder in OnTarget Laboratories LLC. Dr. Nie discloses a relationship as a consultant for Spectropath Inc.

five-year survival by 10 fold compared to patients who do not undergo surgery(1–3). However, despite a “curative” complete surgical resection, 10–20% of patients who undergo pulmonary surgery relapse due to tumor cells that remain at the margin and then re-popluate(1–4). During an operation, surgeons make subjective decisions about the margin status based on their experience, visual review and finger palpation. However, this is historically inaccurate and can lead to inadequate resections and positive surgical margins(5).

Intraoperative molecular imaging has been proposed as a novel technology to augment a surgeons’ visual information in the operating room(6). A targeted optical contrast agent in conjunction with an imaging device can be used during surgery to identify remaining tumor cells after removing a solid tumor(7). Molecular imaging optically enhances the visual information provided to the surgeon, does not use ionizing radiation, and gives real-time information in the operating room. In the last several years, others have become interested in using intraoperative molecular imaging to locate metastatic lesions in ovarian and colorectal cancer(6, 8, 9). However, this technology has not been applied to identify surgical margins.

The folate receptor (FR) is a highly expressed target in pulmonary adenocarcinomas. Folate, a B vitamin (molecular weight 440), plays a key role in metabolic processes involved in DNA and RNA synthesis, epigenetic processes, cellular proliferation, and survival of lung adenocarconomas(10). There are 4 members of the folate receptor family, though only FRα and FRβ bind folate with high affinity. FRα is naturally expressed at the basal surface of polarized alveolar epithelial cells, thus these cells do not bind serum folate(11–13). On the other hand, approximately 80–90% of lung adenocarcinomas express apical luminal FRα (1–3 million receptors/cancer cell) and bind serum folate 10^3–10^4 times more avidly than normal pulmonary epithelial cells(14–16[1]). Thus, FRα provides a reasonable molecular target on pulmonary adenocarcinomas for diagnostic purposes.

The goal of this study is to develop the preclinical data for EC17 which is a folate-based optical contrast agent targeting FRα to inspect the margins after resecting pulmonary adenocarcinomas. In murine models, we establish the optimal timing and dosage of EC17 for imaging adenocarcinomas. We then studied the biodistribution following systemic EC17 injection at various time points. Next, we compare surgical resection using standard techniques of visual inspection and manual palpation for detecting positive margins to molecular imaging. Based on these findings, we examine whether this approach is feasible during pulmonary resection in patients with lung cancer.

Materials and Methods

Cell Lines

The murine lung cancer cell line, TC1, was derived from mouse lung epithelial cells immortalized with HPV-16 E6 and E7 and transformed with the c-Ha-ras oncogene. The spontaneously metastatic murine lung cancer line, LKR, was derived from a pulmonary tumor explanted from an activated KrasG12D mutant mouse that had been induced in an F1 hybrid of 129Sv.J and C57BL/6. The metastatic NSCLC cell line, murine Lewis lung carcinoma (LLC), was obtained from American Type Culture Collection (Manassas, VA).

AE17 is an asbestos-derived murine mesothelioma cell line (kindly provided by Steven Albelda, University of Pennsylvania). KB is a human carcinoma cell line originally believed to be of oropharyngeal origin, but was eventually found to be a derivative of the human papilloma cell line, HeLa. The murine malignant mesothelioma cell line, AB12, was derived from an asbestos-induced tumor and has been previously described in detail[2]. The murine esophageal carcinoma cell line, AKR, was derived from mouse esophageal squamous epithelia with cyclin D1 over-expression via Epstein-Barr virus ED-L2 promoter in p53-deficient genetic backgrounds.

AB12, LKR, AKR, and LLC cell lines were cultured and maintained in high-glucose DMEM (Dulbecco's Modified Eagle's Medium, Mediatech, Washington DC) supplemented with 10% fetal bovine serum (FBS; Georgia Biotechnology, Atlanta, GA), 1% penicillin/streptomycin, and 1% glutamine. TC1, AE17, and KB cell lines were cultured in folate-deficient RPMI (RPMI 1640 Medium, Mediatech, Washington DC), 10% FBS, 1% penicillin/streptomycin, and 1% glutamine. Cell lines were regularly tested and maintained negative for *Mycoplasma spp*

EC17

Folate hapten (vitamin B9) and fluorescein isothiocyanate (FITC) are conjugated through an ethylenediamine spacer to produce EC17 ($C_{42}H_{34}N_{10}Na_2O_{10}S$). EC17 has a molecular weight of 917 kDa. FITC is a derivative of fluorescein functionalized with an isothiocyanate reactive group. FITC is excited by a 465–490 nm wavelength light source and emits light in the 520–530 nm range which falls within the visible light spectrum. The folate-FITC conjugate forms a negatively charged fluorescent molecule that specifically targets cell-surface FRα and is subsequently internalized into the cytoplasm(17, 18). All vials of EC17 were supplied by On Target Laboratories, Inc. (West Lafayette, IN). For the human study, 0.1 mg/kg of EC17 was dissolved in 10 mL of normal saline and injected over 10 minutes via peripheral vein two hours prior to operation. After injection of EC17, all patients were monitored for 30 minutes after injection for evidence of adverse reaction.

Fluorescent imaging

Macroscopic surgical fluorescent imaging was performed using the FloCam (BioVision, Exeter, PA, USA) or the Artemis Fluorescence Imaging system (Quest ® Medical Imaging, the Netherlands). The FloCam was used for animal imaging and is a research imaging system capable of dual imaging with white light (λex 490 nm). The Artemis Fluorescence Imaging System similarly emits light at 490 nm and absorbs light at 530 nm and was used for our pilot human trial. Positive controls included diluted dye and negative controls were muscle tissue to calibrate the system in each experiment. Of note, in order to control for the auto-fluorescence present in the white fur of our mice, we linearly increased fluorescent image contrast on the FloCam. Images were obtained when the auto-fluorescence was no longer detectable in the fur but was still clearly present in the tumor. All images were photo documented and taken in triplicate.

Murine flank tumor models

NOD scid gamma mice were injected subcutaneously in the flank with $1e^6$ KB tumor cells. Tumor cells for subcutaneous injections were suspended in 100μL PBS. Tumor volume was calculated using the formula $(3.14 \times \text{long-axis} \times \text{short-axis}^2)/6$. Mice were fed an exclusively folate deficient chow (Harlan® Laboratories) on the day of inoculation until end-point.

Initially, 5 tumor-bearing mice underwent bolus tail-vein injections at each EC17 dose (0.01 mg/kg, 0.05 mg/kg, 0.1 mg/kg, 0.25 mg/kg, 0.5 mg/kg) for a total of 25 mice. They were then anesthetized with intramuscular ketamine (80 mg/kg) and xylazine (10 mg/kg) and subjected to fluorescent imaging at 520 nm at 5 min, 30 min, 60 min, 120 min, 4 hr, 8hr and 24hr after tracer injection. After the 24-hour time point, all animals were euthanized and organs were examined for histopathology.

After establishment of ideal EC17 dose and injection timing, 6 mice were given 0.1 mg/kg of EC17 via tail vein injection. In order to assess the tissue distribution of EC17, each mouse was euthanized and vital organs were removed for imaging at several time points (2hr, 8hr, 24hr, 48hr, 5 days and 7 days).

An additional 120 mice with similarly established flank tumors underwent surgery using an established resection model(19). Surgery was performed when tumors reached ~ 250 mm^3. Mice were injected with 0.1 mg/kg of EC17 via tail vein. Two hours after injection, mice were anesthetized with intramuscular ketamine (80 mg/kg) and xylazine (10 mg/kg), shaved, and then sterilized prior to surgery. A 1-to-2 cm incision was made adjacent to the tumor and the tumor was removed using standard blunt and sharp dissection techniques. The surgeon intentionally left approximately 1 mm of tumor hidden within the fur and soft tissue of the surgical margin in 60 of the 120 mice. Next, two independent investigators inspected the surgical field in an attempt to discover retained tumor. The first investigator was allowed to use his hands and eyes only, while the second investigator used these traditional methods as well as fluorescence imaging. Each true positive wound bed (determined by the testing surgeon) as well as suspected positive margins chosen by each investigator were biopsied.

Human lung adenocarcinoma study design

Three human patients with a preoperative diagnosis of lung adenocarcinoma were enrolled in a pilot trial using intraoperative molecular imaging. The clinical study was approved by the University of Pennsylvania Institutional Review Board and the Philadelphia Veterans Affairs Medical Center, and patients underwent informed written consent. Prior to operation, all patients underwent computed tomography (CT) scanning and an ^{18}fluorodeoxygluocse positron emission tomography (^{18}FDG-PET) scan to rule out extrathoracic metastatic disease. Tissue biopsy was obtained in each case and biopsies were confirmed adenocarcinoma by a specialized thoracic pathologist at our institution. Additionally, the lung samples were stained and confirmed positive for FRα using immunohistochemistry. None of these patients received chemotherapy or radiation prior to operation. All patients were asked to stop folate-containing vitamins one week prior to surgery.

Two hours prior to surgery, patients were administered 0.1 mg/kg of EC17 via peripheral antecubital vein. Twenty-five mg of benadryl was administered pre-infusion as a prophylactic measure. Registered nurses monitored vital signs every 5 minutes throughout infusion time and for an additional 30 minutes post infusion. With any signs of adverse events, the nurses were instructed to discontinue the infusion immediately. All patients left the clinical research center and were transported to the preoperative area in a wheelchair. Intraoperatively, patients underwent standard anesthesia and single lung ventilation. Access was gained to the involved lung via standard thoracotomy. Once the tumor was localized using traditional methods, the operating room lights were switched off, and the fluorescent imaging system was sterily draped and positioned above the chest using a custom designed gautry device (BioMediCon, Moorestown, NJ). The tumor was imaged on the deflated lung and photo-documented by fluorescence and white light *in situ*. Following tumor resection, before submission to pathology, all specimens were re-imaged *ex vivo* to provide close-up molecular imaging of the tumor. Additionally, we imaged the wound bed to assess for retained fluorescence following tumor resection. Final specimens were reviewed by a specialized lung pathologist.

Fluorescence Microscopy

Fluorescence microscopy was performed using an Olympus IX51 fluorescent microscope equipped with a fluorescein specific filter set (Chroma® 49012). In order to quantitate the tissue and tumor fluorescence, we used region-of-interest software and HeatMap plugin within ImageJ (http://rsb.info.nih.gov/ij/; public domain free software developed by National Institutes of Health). Background readings were taken from adjacent muscle and subcutaneous tissue in order to generate a tumor-to-background ratio (TBR). All readings were done in triplicate.

Immunohistochemical Staining

Surgical margin specimens were harvested and bisected with one-half either placed in Tissue-Tek OCT and stored at −80°C or in formalin for paraffin sectioning. Frozen tumor sections were prepared as previously described(20). To detect FRα and FITC, the monoclonal mouse antibody Mab343 (Morphotek Inc., PA) and monoclonal mouse antibody Mab10257 (Abcam ®) were used, respectively.

Statistics

After measuring tumor-to-background ratio (TBR) of each tumor in triplicate as previously described, mean TBR was calculated for each tumor. The mean TBR of each murine flank tumor was then averaged at each time point and was evaluated for significant difference using analysis of variance (ANOVA). Statistics were considered significant at p values ≤ 0.05. Additionally, sensitivity, specificity, positive predictive value and negative predictive value were calculated for both investigators involved in the evaluation of surgical margins. All calculations were performed in Excel (Microsoft ®).

Results

Cancer cell lines express FRα and uptake a folate-targeted fluorophore *in vitro*

In order to identify human and murine cancer cell lines that express FRα, 7 readily available murine and human cell lines (AB12, AKR, LKR, TC1, LLC, KB, and AE17) were selected for immunohistochemistry. Our staining showed that KB and AE17 cells avidly expressed *FR*α (Fig. 1a).

To demonstrate that the folate-fluorophore conjugate could act as a specific ligand for tumor cells, we tested it on KB and AE-17 cell lines, as well as TC1 cells to be used as a negative control. The EC17 conjugate was incubated with each cell line for 4 hours. After washing the stained cells with PBS to remove free dyes, the cells were imaged using fluorescence microscopy. Dye uptake was seen uniformly in KB and AE17 cell lines (Fig. 1b). Staining localized predominately to the cell surface, with KB cells showing the highest tumor-to-background ratio (TBR) (Fig. 1d).

To further confirm that the cell-bound tracer was the source of the fluorescence, the tumor cells were stained with anti-fluorescein immunoglobulin. This showed strong staining for FITC on both KB and AE17 cells (>80% tumor cells) (Fig. 1c).

In vivo pharmacokinetics of EC17 in murine xenografts

Next, we sought to determine the optimal dose and time to systemically deliver EC17 for optimal TBR in xenografts. We chose to use KB flank tumors for this experiment because of the higher density of FRα noted on immunohistochemistry as well as the superior TBR of this cell line. Flank KB xenografts were established in 25 NOD/SCID/Gama mice. When tumors reached 250 mm^3, the animals underwent tail vein injection at five different doses of EC17 (0.01 mg/kg, 0.05 mg/kg, 0.1 mg/kg, 0.25 mg/kg, 0.5 mg/kg) and subjected to fluorescent imaging λex 490 nm at various time points (5 min, 30 min, 60 min, 120 min, 4hr, 8hr and 24hr).

All animals survived the study. The soft tissue fluorescence noted within the extremities and tail (4.10 a.u. +/− 0.32) was brightest within 10 minutes of injection. The tumor fluorescence (4.12 a.u. +/− 0.41) peaked two hours after injection. The dye was found to accumulate in the tumor for up to 4 hours, and signal decreased to background levels (0.12 a.u. +/− 0.03) by 24 hours (Fig. 2a). TBRs were not significantly different at a dose of 0.1 mg/kg and above, thus we chose 0.1 mg/kg the lowest most effective dose (Fig. 2b). The mean TBR of mice injected with 0.1 mg/kg at the two-hour time period was 3.9 +/− 0.2 (IQR 3.8–4.1). The presence of cancer cells was confirmed in all mice using histopathological analysis of tumor sections by H&E (Fig. 3a), and the presence of FRα and localized EC17 was confirmed in 10 mice using both FRα IHC (Fig. 3b) and fluorescence microscopy (Fig. 3c).

Biodistribution and Uptake of EC17

After the final 24-hour time point, each animal was euthanized and organs were assessed for signs of toxicity. No obvious toxicity was observed at any dose, which was confirmed with histopathology (Fig. 4a). In order to assess tissue distribution of EC17, an additional 6 mice

received 0.1 mg/kg EC17 and organs were harvested at various time points (2 hr, 8 hr, 24 hr, 2 days, 5 days and 7 days) (Fig. 4b). Fluorescent signal was noted in the stomach and small bowel in all mice. No fluorescence was noted in any other organs, including brain, lungs, heart, kidneys, spleen, and liver. No tissue:background ratio greater than 1.0 was measured for any organs other than the bowel and stomach when compared to muscle as background. Time-dependent dye clearance from normal mouse organs showed minimal dye in the bowel 24 hours after injection, and there was no fluorescence remaining after 48 hours.

Residual tumor in the surgical bed fluoresces after incomplete resection

In order to determine if fluorescent imaging could detect residual tumor deposits after surgery, flank KB xenografts were established in NOD scid gamma mice. 120 animals in 5 separate experiments were administered EC17 and underwent our previously described resection model. After both investigators had independently assessed the wound, any areas deemed suspicious by either investigator, as well as the known positive margins established by the primary surgeon, were removed for histology.

The first investigator, using visual inspection and manual palpation, accurately detected 18 residual tumors and falsely identified 4 mice as having positive margins. The second investigator who had molecular imaging at his disposal to inspect the wound detected all 18 margins identified by the first investigator as well as an additional 30 animals with positive margins, for a total of 48 positive margins (Fig. 5a). The residual fluorescent deposits in the wound had an intensity ranging from 3.54 to 4.34 a.u. (IQR 3.78–4.12 a.u.); the mean background fluorescence in these cases was 1.01 a.u. (IQR 0.89–1.22 a.u.).

TBR of these residual tumor deposits was 4.0 +/− 0.2 (IQR 3.8–4.1) which was not significantly different than the primary tumors ($p=0.91$). The second investigator did not have any false positives, e.g., fluorescent imaging did not incorrectly visually enhance normal tissues in the wound bed. All biopsies were sectioned and stained by H&E to evaluate for residual tumor cells (Fig. 5b). The twelve remaining wound beds with residual tumor cells that were not located by either investigator were confirmed to have tumor cells on H&E.

In total, 60 mice had positive surgical margins: 18 were discovered by visual inspection and manual palpation, 48 were found by intraoperative molecular imaging adjunct, and 12 were missed by both modalities. Intraoperative molecular imaging detected a statistically greater proportion of positive surgical margins compared to manual palpation and visual inspection (80% vs. 30%, $p<0.01$). Overall, fluorescent imaging had a sensitivity of 80%, specificity of 100%, positive predictive value of 100%, and negative predictive value of 83%. Visual inspection and manual palpation had a sensitivity of 30%, specificity of 90%, positive predictive value of 82%, and negative predictive value of 56% (Fig. 5c).

Lung adenocarcinomas can be identified by fluorescent imaging during pulmonary resection

Based on these results, three patients with known pulmonary adenocarcinomas were enrolled in a pilot study for folate-based intraoperative molecular imaging. There were no side effects noted during or after EC17 infusion in any of the patients, including changes in subjective

complaints, vital signs or physical exam. One representative patient and her images are reviewed here: a 64 year old female initially presented with a cough and chest radiography showed a 3 cm PET-positive left upper lobe lesion with a standard uptake value on ^{18}FDG-PET of 5.2 (Fig. 6a). Subsequent biopsy was consistent with pulmonary adenocarcinoma, and immunohistochemistry confirmed the presence of FRα receptors. This patient was deemed a suitable candidate for thoracotomy and pulmonary resection. Approximately two hours before surgery, the patient was given 0.1 mg/kg of EC17 without complication.

Following thoracotomy and tumor localization with traditional palpation and inspection, molecular imaging was used *in vivo*, which showed a fluorescent tumor with an intensity of 3.64 a.u., background intensity 1.10 a.u., and TBR of 3.3. (Fig. 6b). After removing the tumor from the patient, the specimen was re-imaged on the back table *ex vivo*, and the tumor was bisected without affecting the pathologists' ability to identify margins. Resection margins were noted to be negative for fluorescence with a sharp demarcation of fluorescent signal absent from the surrounding lung parenchyma. The wound bed was then re-imaged *in vivo* and noted to be free of any residual fluorescence (Fig. 6c). FRα immunohistochemistry confirmed the upregulation of the folate receptor on the tumor cells, and fluorescence microscopy confirmed tumor cell localization of FITC (Fig. 6d). Final pathology confirmed the tumor to be an adenocarcinoma.

The two additional patients were 62 and 71 years old. Their tumors were between 2 and 3 cm in size and were also markedly fluorescent both with a TBR of 3.6. Of note, some areas of autofluorescence were noted on the bronchi each patient. In each case, the areas of autofluorescence were far enough away from the primary tumor to not obscure the lesion itself. We did not evaluate the lymph nodes for fluorescence.

In all 3 pilot cases, there was no residual fluorescence in the wound bed. All patients are at least one year from the time of surgery and repeat imaging has shown no evidence of local recurrence.

Discussion

The most important predictor for a successful lung cancer operation is complete removal of the tumor at the time of surgery with no residual tumor cells ("negative surgical margins.") (22). However, it can be difficult for surgeons to tell whether they have obtained negative margins as they traditionally rely on visual and tactile examination of the wound bed in the operating room. We proposed using intraoperative molecular imaging with a targeted fluorescent contrast agent to aid in inspection of the wound in patients with lung adenocarcinoma.

We found that doses higher than 0.1 mg/kg did not significantly improve TBR, and therefore this dose was chosen as our lowest optimal dose for humans. In our pharmacokinetic studies, we found the optimal time and dose to systemically inject EC17 was 2 hours and 0.1 mg/kg, respectively. We found no evidence of tissue toxicity in any of our studies. Our murine margin study showed significantly higher rate of positive margin detection when intraoperative molecular imaging was utilized in addition to traditional means. Additionally,

molecular imaging did not interrupt our surgeon's ability to use visual inspection and finger palpation, and it is an important adjunct to improve outcomes.

In this study, systemically injected EC17 was used as the tracer for identifying pulmonary adenocarcinomas. FRα is a folate-binding protein overexpressed on several epithelial malignancies, including lung and ovarian cancer, and therefore provides a target for tumor localization. Fluorescent molecules, like FITC, can be tagged to a variety of other ligands allowing for increased specificity to various tissue and tumor types. Currently, there are dozens of ligand-based tracers being evaluated in experimental models(23–25). For example, Sturm *et al* who presented a tumor-specific probe by binding the ASYNYDA peptide to FITC (ASY*-FITC) for the intraoperative imaging of early stage esophageal adenocarcinoma(26). Additionally, urokinase plasminogen activator (uPA) labeled with NIR dye allows intraoperative margin imaging of mice bearing orthotopic human breast or pancreatic tumors(27). Similarly, there is an ongoing phase 1 clinical trial involving intraoperative imaging of breast cancer using bevacizumab (targeted to VEGF) conjugated to the IRDye 800 CW(28).

Intraoperative molecular imaging possesses many useful properties that make it a potentially useful tool in surgical decision-making. First, this technology is rapidly and readily interpretable because it is optical. The information is obtained real-time and does not involve ionizing radiation. We observed that molecular imaging increased the surgeons' confidence and diagnostic accuracy which led to shorter operative times. Based on our observations, we believe this will be particularly useful for minimally invasive procedures and it may reduce the need to convert to open thoracotomy in the case of difficult to locate tumors. Intraoperative molecular imaging of pulmonary adenocarcinomas may increase detection of residual disease and thereby allow for a complete resection. This should decrease the need for postoperative radiation and provide more accurate intraoperative staging as well as possibly improved survival.

Although the majority of NSCLC are treated with lobectomy or pneumenectomy, this varies largely depending on surgeon. Additionally, the incidence of wedge resection for small pulmonary carcinomas is increasing, and in these cases, negative margins are important for oncologic control. In cases in which lobectomy or pneumenectomy are planned, intraoperative molecular imaging could potentially help with detecting small tumors that are difficult to visualize and palpate. Additionally, this technology may also be helpful in diagnosis. Of course, clinical trials need to be conducted to test these claims. This study provides proof of principle of the successful intraoperative molecular imaging of pulmonary adenocarcinomas.

Not all of the residual tumor deposits left by the surgeon in our murine model were discovered with fluorescence imaging. There are several reasons why this may have occurred. It is possible that after resecting the tumor, the piece left behind was so small that the camera lacked sufficient resolution to detect such a small area of fluorescence. Additionally, with the manipulation of the tumor, it is possible that the tracer was manually removed. This seems less likely, however, because EC17 is receptor bound. It is also possible that upon hiding the residual tumor, the tumor was placed too deep in the wound

bed so that the camera/EC17 combination lacked sufficient depth of penetration. This could be explained by the suboptimal depth of penetration of tracers within the visible spectrum. For example, while near-infrared light can penetrate into tissue and reflect back to the surface without being significantly absorbed, visible light is greatly scattered and absorbed within the depth of just a few hundred microns. This makes NIR a better spectral region for performing fluorescence imaging on thick tissue[3].

There were several limitations noted while carrying out this study. As a result of imaging within the visible light spectrum, there was significant autofluorescence of natural fluorophores in the hair of white-furred mice. However, because the muscle did not fluoresce, the tumors were easily distinguished from background once exposed, which allowed for accuracy of our margin study. Another limitation is the potential lack of translatability between our mouse model and human lung cancer patients. Mouse flank tumors are homogenous and well defined, and the surrounding subcutaneous tissue is arguably less complex than lung parenchyma. Although promising, a larger human clinical trial is underway to determine efficacy.

Acknowledgments

Funding

This work was supported by the National Institutes of Health RO1 CA163256.

References

1. Aliperti LA, Predina JD, Vachani A, Singhal S. Local and systemic recurrence is the Achilles heel of cancer surgery. Ann Surg Oncol. 2011; 18:603–607. [PubMed: 21161729]
2. Osarogiagbon RU, Phelps G, McFarlane J, Bankole O. Causes and consequences of deviation from multidisciplinary care in thoracic oncology. J Thorac Oncol. 2011; 6:510–516. [PubMed: 21258245]
3. Detterbeck FC, Tanoue LT, Boffa DJ. Anatomy, biology and concepts, pertaining to lung cancer stage classification. Zhongguo Fei Ai Za Zhi. 2010; 13:1–8. [PubMed: 20672696]
4. Pisters KM, Le Chevalier T. Adjuvant chemotherapy in completely resected non-small-cell lung cancer. J Clin Oncol. 2005; 23:3270–3278. [PubMed: 15886314]
5. Vaidya A, Hawke C, Tiguert R, Civantos F, Soloway M. Intraoperative T staging in radical retropubic prostatectomy: is it reliable? Urology. 2001; 57:949–954. [PubMed: 11337301]
6. Singhal S, Nie S, Wang MD. Nanotechnology applications in surgical oncology. Annu Rev Med. 2001; 61:359–373.
7. Madajewski B, Judy BF, Mouchli A, Kapoor V, Holt D, Wang MD, Nie S, Singhal S. Intraoperative near-infrared imaging of surgical wounds after tumor resections can detect residual disease. Clin Cancer Res. 2012; 18:5741–5751. [PubMed: 22932668]
8. van der Vorst JR, Schaafsma BE, Hutteman M, Verbeek FP, Liefers GJ, Hartgrink HH, Smit VT, Lowik CW, van de Velde CJ, Frangioni JV, Vahrmeijer AL. Near-infrared fluorescence-guided resection of colorectal liver metastases. Cancer. 2013; 119:3411–3418. [PubMed: 23794086]
9. van Dam GM, Themelis G, Crane LM, Harlaar NJ, Pleijhuis RG, Kelder W, Sarantopoulos A, de Jong JS, Arts HJ, van der Zee AG, Bart J, Low PS, Ntziachristos V. Intraoperative tumor-specific fluorescence imaging in ovarian cancer by folate receptor-alpha targeting: first in-human results. Nat Med. 2011; 17:1315–1319. [PubMed: 21926976]
10. Kelemen LE. The role of folate receptor alpha in cancer development, progression and treatment: cause, consequence or innocent bystander? Int J Cancer. 2006; 119:243–250. [PubMed: 16453285]
11. Low PS, Antony AC. Folate receptor-targeted drugs for cancer and inflammatory diseases. Adv Drug Deliv Rev. 2004; 56:1055–1058. [PubMed: 15094205]

12. Low PS, Henne WA, Doorneweerd DD. Discovery and development of folic-acid-based receptor targeting for imaging and therapy of cancer and inflammatory diseases. Acc Chem Res. 2008; 41:120–129. [PubMed: 17655275]
13. Xia W, Low PS. Folate-targeted therapies for cancer. J Med Chem. 2010; 53:6811–6824. [PubMed: 20666486]
14. O'Shannessy DJ, Yu G, Smale R, Fu YS, Singhal S, Thiel RP, Somers EB, Vachani A. Folate receptor alpha expression in lung cancer: diagnostic and prognostic significance. Oncotarget. 2012; 3:414–425. [PubMed: 22547449]
15. Lu Y, Sega E, Leamon CP, Low PS. Folate receptor-targeted immunotherapy of cancer: mechanism and therapeutic potential. Adv Drug Deliv Rev. 2004; 56:1161–1176. [PubMed: 15094213]
16. Low PS, Kularatne SA. Folate-targeted therapeutic and imaging agents for cancer. Curr Opin Chem Biol. 2009; 13:256–262. [PubMed: 19419901]
17. Davis MR, Manning LS, Whitaker D, Garlepp MJ, Robinson BW. Establishment of a murine model of malignant mesothelioma. International journal of cancer. Journal international du cancer. 1992; 52(6):881–886. [PubMed: 1459729]
18. Lu Y, Xu LC, Parker N, Westrick E, Reddy JA, Vetzel M, Low PS, Leamon CP. Preclinical pharmacokinetics, tissue distribution, and antitumor activity of a folate-hapten conjugate-targeted immunotherapy in hapten-immunized mice. Mol Cancer Ther. 2006; 5:3258–3267. [PubMed: 17172429]
19. Lu Y, Low PS. Folate targeting of haptens to cancer cell surfaces mediates immunotherapy of syngeneic murine tumors. Cancer Immunol Immunother. 2002; 51:153–162. [PubMed: 11941454]
20. Predina JD, Judy B, Fridlender ZG, Aliperti LA, Madajewski B, Kapoor V, Cheng G, Quatromoni J, Okusanya O, Singhal S. A positive-margin resection model recreates the postsurgical tumor microenvironment and is a reliable model for adjuvant therapy evaluation. Cancer Biol Ther. 2012; 13:745–755. [PubMed: 22617772]
21. Judy BF, Aliperti LA, Predina JD, Levine D, Kapoor V, Thorpe PE, Albelda SM, Singhal S. Vascular endothelial-targeted therapy combined with cytotoxic chemotherapy induces inflammatory intratumoral infiltrates and inhibits tumor relapses after surgery. Neoplasia. 2012; 14:352–359. [PubMed: 22577350]
22. Fedor D, Johnson WR, Singhal S. Local recurrence following lung cancer surgery: incidence, risk factors, and outcomes. Surg Oncol. 2013; 22:156–161. [PubMed: 23702313]
23. Gomez DR, Komaki R. Postoperative radiation therapy for non-small cell lung cancer and thymic malignancies. Cancers (Basel). 2012; 4:307–322. [PubMed: 24213242]
24. Trajkovic-Arsic M, Mohajerani P, Sarantopoulos A, Kalideris E, Steiger K, Esposito I, Ma X, Themelis G, Burton N, Michalski CW, Kleeff J, Stangl S, Beer AJ, Pohle K, Wester HJ, Schmid RM, Braren R, Ntziachristos V, Siveke JT. Multimodal molecular imaging of integrin alphavbeta3 for in vivo detection of pancreatic cancer. J Nucl Med. 2014; 55:446–451. [PubMed: 24549287]
25. Metildi CA, Kaushal S, Pu M, Messer KA, Luiken GA, Moossa AR, Hoffman RM, Bouvet M. Fluorescence-guided surgery with a fluorophore-conjugated antibody to carcinoembryonic antigen (CEA), that highlights the tumor, improves surgical resection and increases survival in orthotopic mouse models of human pancreatic cancer. Ann Surg Oncol. 2014; 21:1405–1411. [PubMed: 24499827]
26. Hiroshima Y, Maawy A, Metildi CA, Zhang Y, Uehara F, Miwa S, Yano S, Sato S, Murakami T, Momiyama M, Chishima T, Tanaka K, Bouvet M, Endo I, Hoffman RM. Successful fluorescence-guided surgery on human colon cancer patient-derived orthotopic xenograft mouse models using a fluorophore-conjugated anti-CEA antibody and a portable imaging system. J Laparoendosc Adv Surg Tech A. 2014; 24:241–247. [PubMed: 24494971]
27. Sturm MB, Joshi BP, Lu S, Piraka C, Khondee S, Elmunzer BJ, Kwon RS, Beer DG, Appelman HD, Turgeon DK, Wang TD. Targeted imaging of esophageal neoplasia with a fluorescently labeled peptide: first-in-human results. Sci Transl Med. 2013; 5:184ra161.
28. Yang L, Sajja HK, Cao Z, Qian W, Bender L, Marcus AI, Lipowska M, Wood WC, Wang YA. uPAR-targeted optical imaging contrasts as theranostic agents for tumor margin detection. Theranostics. 2013; 4:106–118. [PubMed: 24396518]

29. Chi C, Du Y, Ye J, Kou D, Qiu J, Wang J, Tian J, Chen X. Intraoperative imaging-guided cancer surgery: from current fluorescence molecular imaging methods to future multi-modality imaging technology. Theranostics. 2014; 4:1072–1084. [PubMed: 25250092]

30. Jacques SL. Optical properties of biological tissues: a review. Physics in medicine and biology. 2013; 58(11):R37–61. [PubMed: 23666068]

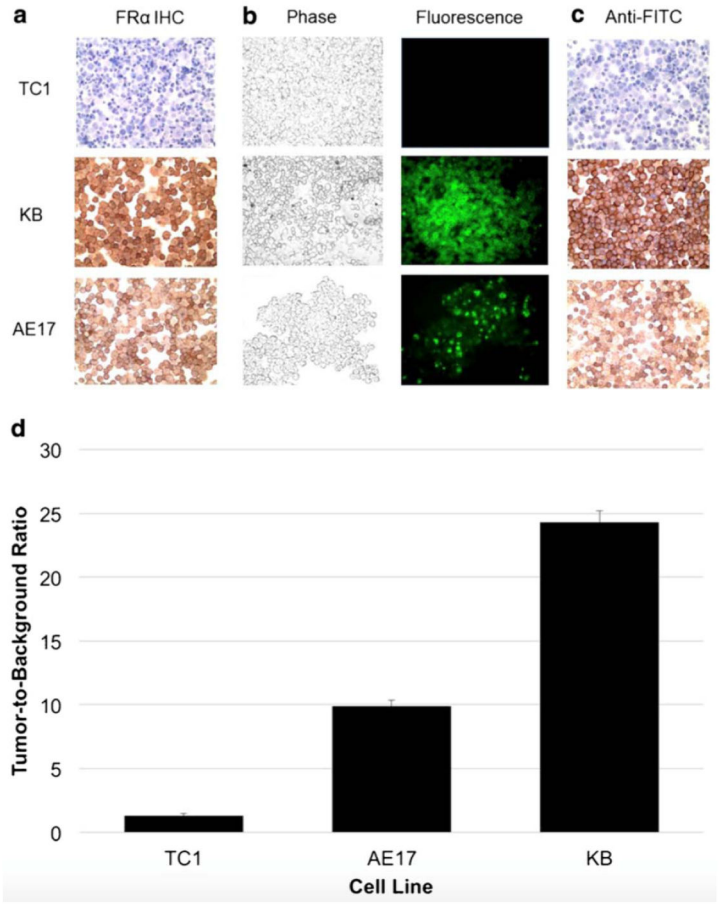

Figure 1.

EC17 detection of murine and human cell lines. A.) KB and AE-17 cell lines display positive *FR*α immunohistochemical staining unlike TC1. B.) EC17 staining of KB and AE-17 cell lines was confirmed by fluorescence microscopy and C.) anti-FITC immunohistochemical staining. D.) Mean TBR of TC1, AE17 and KB cell lines stained with EC17.

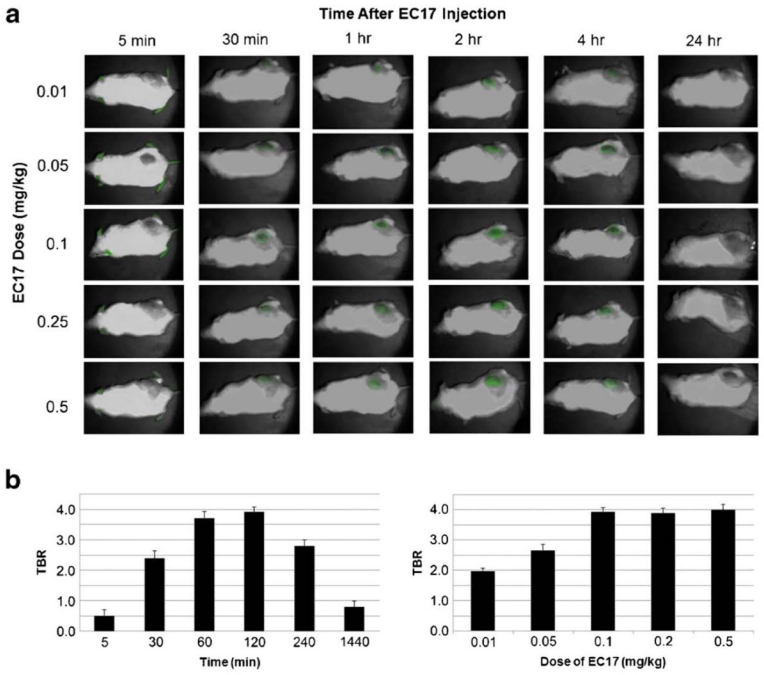

Figure 2.

A.) Fluorescence overlay images of KB flank tumors after varying doses of systemically injected EC17 at several different time points after injection (8hr time point not shown). B.) EC17 injection resulted in peak tumor tumor-to-background ratios (TBR) 2 hours after injection. No significant increase in TBR was seen at doses higher than 0.1 mg/kg.

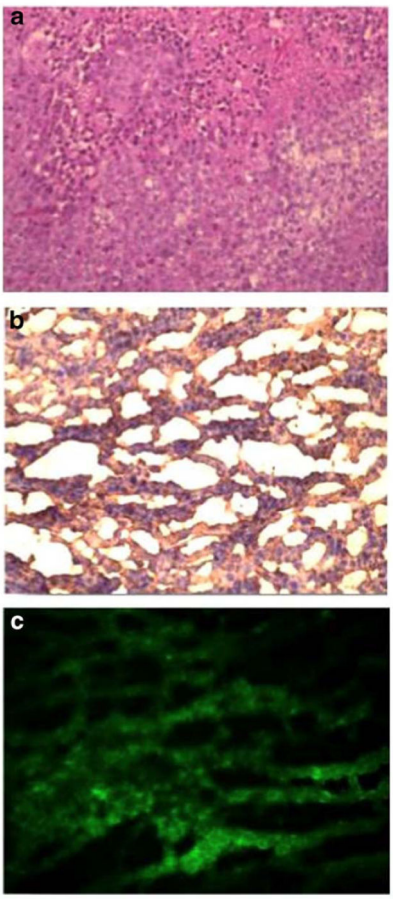

Figure 3.

EC17 can detect murine flank tumors. Flank tumors were confirmed by A.) H&E and shown to be positive for *FR*α by B.) immunohistochemical staining and C.) fluorescence microscopy.

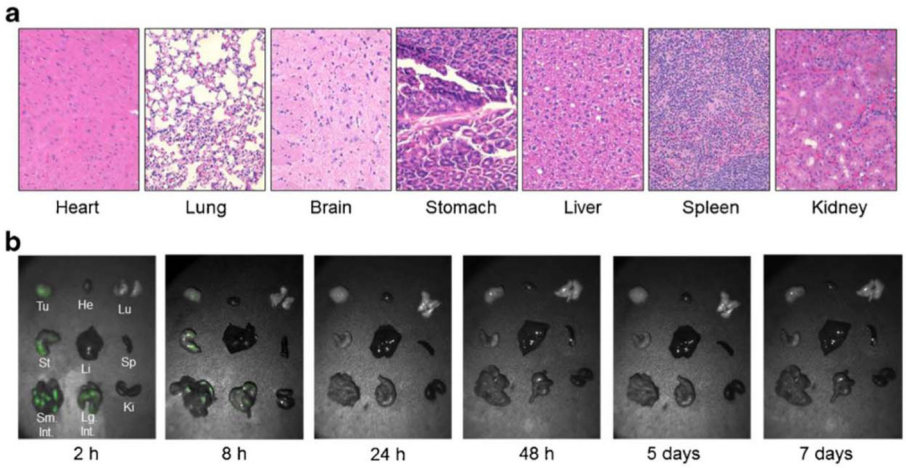

Figure 4.

Effect of EC17 on vital organs. A.) No evidence of histopathology seen in the vital organs of mice 24 hours after 0.1 mg/kg systemic injection of EC17. B.) Biodistribution of EC17 at various time points after injection as seen with fluorescent imaging. Fluorescence noted in the GI tract and is no longer evident by 48 hours.

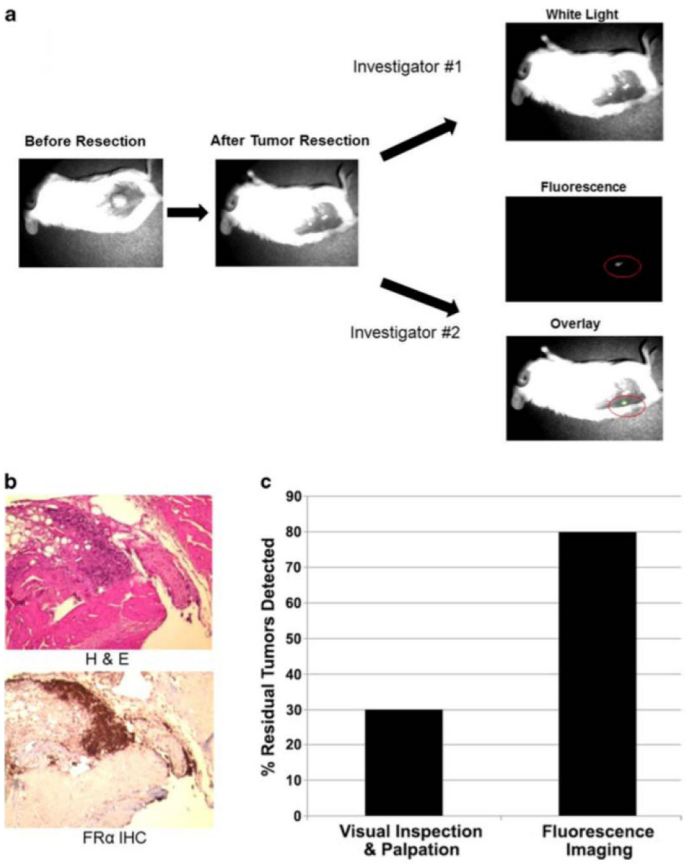

Figure 5.

A.) Operative schematic of KB flank tumor resection and assessment of margins using traditional inspection versus intraoperative molecular imaging. EC17 can detect positive surgical margins. B.) H&E and immunohistochemical staining confirmed *FR*α positive tumor at the surgical margin. C.) Detection of positive surgical margins was superior by combining fluorescent molecular imaging with visual inspection and palpation ($p < 0.01$).

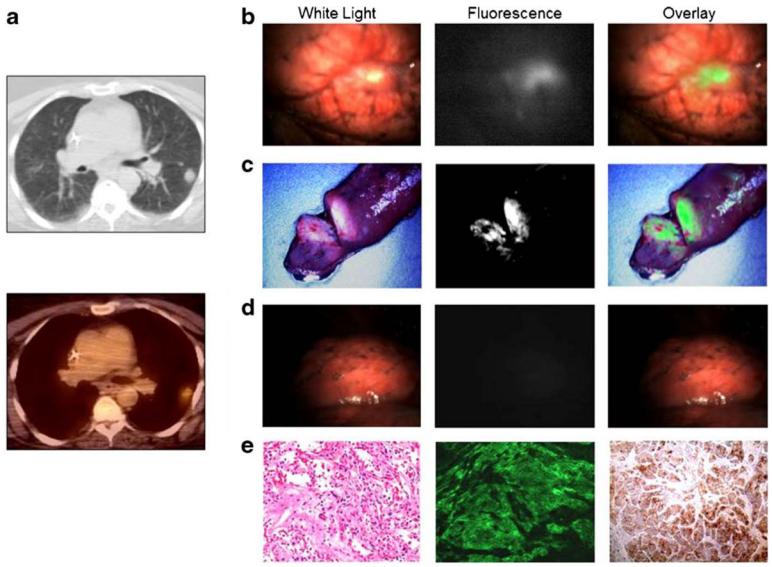

Figure 6.

EC17-based intraoperative fluorescent imaging can identify human adenocarcinomas. A.) CT and PET scan of 3 cm left upper lobe adenocarcinoma prior to pulmonary resection. B.) Intraoperative fluorescent imaging was performed with clear tumor delineation. C.) The wound bed was inspected with λex 490 nm and demonstrated no residual fluorescence at the surgical margins. D.) FRα upregulation was confirmed by fluorescence microscopy and immunohistochemical staining.